CARBON letters

Original Articles
Carbon Letters Vol. 22, 14-24 (2017)

Kinetic and multi-parameter isotherm studies of picric acid removal from aqueous solutions by carboxylated multi-walled carbon nanotubes in the presence and absence of ultrasound

Soheila Gholitabar and Hasan Tahermansouri*

Department of Chemistry, Ayatollah Amoli Branch, Islamic Azad University, Amol 46351-43358, Iran

Article Info

Received 9 June 2016
Accepted 8 February 2017

***Corresponding Author**
E-mail: h.tahermansuri@iauamol.ac.ir
Tel: +981143217076

Open Access

DOI: http://dx.doi.org/10.5714/CL.2017.22.014

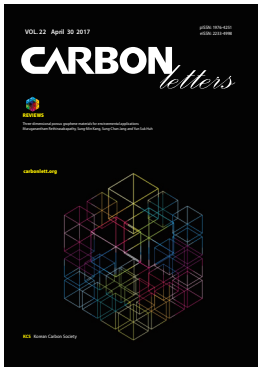

http://carbonlett.org

pISSN: 1976-4251
eISSN: 2233-4998

Abstract

Carboxylated multi-wall carbon nanotubes (MWCNTs-COOH) have been used as efficient adsorbents for the removal of picric acid from aqueous solutions under stirring and ultrasound conditions. Batch experiments were conducted to study the influence of the different parameters such as pH, amount of adsorbents, contact time and concentration of picric acid on the adsorption process. The kinetic data were fitted with pseudo-first order, pseudo-second-order, Elovich and intra-particle diffusion models. The kinetic studies were well described by the pseudo-second-order kinetic model for both methods. In addition, the adsorption isotherms of picric acid from aqueous solutions on the MWCNTs were investigated using six two-parameter models (Langmuir, Freundlich, Tempkin, Halsey, Harkins-Jura, Fowler-Guggenheim), four three-parameter models (Redlich-Peterson, Khan, Radke-Prausnitz, and Toth), two four-parameter equations (Fritz-Schlunder and Baudu) and one five-parameter equation (Fritz-Schlunder). Three error analysis methods, correlation coefficient, chi-square test and average relative errors, were applied to determine the best fit isotherm. The error analysis showed that the models with more than two parameters better described the picric acid sorption data compared to the two-parameter models. In particular, the Baudu equation provided the best model for the picric acid sorption data for both methods.

Key words: carbon nanotube, picric acid, kinetics, ultrasound, adsorption isotherms

1. Introduction

Nitrophenols are used as intermediates in the production of dyes, pigments, preservatives, pesticides, pharmaceuticals and rubber chemicals [1]. Hence, they usually are found in effluent wastes and rivers with input from munitions and textile factories [1,2]. Among the nitrophenols, 2,4,6-trinitrophenol (picric acid), which is synthesized with inherent stability until detonation, has been used in naval ordnance and was common in many other types of ordnance in the early part of this century [3,4]. Due to the various applications of picric acid in dyes, explosives, analytical reagents, germicides, fungicides, tissue fixatives, photochemicals, and pharmaceuticals as well as for the oxidation and etching of iron, steel, and copper surfaces [5], it could enter the water table or environment and effect the health of humans because picric acid is toxic even at low concentrations [6,7]. On the other hand, the World Health Organization (WHO) reported 0.001 mg/L as the permissible phenolic concentration in potable water [8]. In addition, US Environmental Protection Agency issued a permissible limit of 0.1 mg/L in wastewater [9]. Therefore, the removal of phenolic contaminants from aqueous solutions has become a major focus of research and is essential. The adsorption process is one of the major methods for the removal of phenols, nitrophenols and some of their derivatives from aqueous solutions [10]. The advantage of this technic over other methods, such as filtration, chemical precipitation and ion exchange, is that it is generally easy to handle, can be regenerated by a suitable desorption process, is insensitivity to toxic

pollutants and can be used for various situations without a large apparatus [11,12]. In recent years, carbon nanotubes (CNTs) have been used as effective adsorbents for the removal of various types of contaminants including dyes [13], carbon monoxide [14], metal ions [15-17], phenols [18-21], alkanes [22], drugs [23,24] and aromatic compounds [25,26]. This application of CNTs is related to their large surface areas, electrostatic interactions, and shorter equilibrium time compared to other materials. Ultrasound is a very useful tool in surface adsorption because it intensifies the mass transfer process. Hence, many papers have investigated the adsorption of pollutants by various adsorbents under ultrasound conditions [27-29]. Therefore, we decided to improve this work. In this study, carboxylated multi-wall carbon nanotubes (MWCNT-COOH) was used as an efficient adsorbent for the removal of picric acid from aqueous solutions with stirring and ultrasound methods. The four kinetic models, pseudo-first order, pseudo-second-order, Elovich and intra-particle diffusion models and six two-parameter isotherm models (Langmuir, Freundlich, Tempkin, Halsey, Harkins-Jura, Fowler-Guggenheim), four three-parameter equations (Redlich-Peterson, Khan, Radke-Prausnitz, Toth), two four-parameter models (Fritz-Schlunder and Baudu), and one five-parameter equation (Fritz-Schlunder) were examined to obtain sufficient knowledge on the mechanism and rate of the adsorption process of picric acid on the MWCNTs. In fact, the goal of this investigation was to compare stirring and ultrasound methods in the adsorption of picric acid from aqueous solutions by MWCNT-COOH as an adsorbent.

2. Experimental

2.1. Materials and methods

Picric acid (Merck Chemical Inc., USA) and MWCNTs (%95 purity; OD, 30–50 nm; length, 0.5–2 μm; Neutrino Co., Ltd) were purchased and used as received. Analytical reagent-grade chemicals were used as well as deionized water from a Milli-Q system (Millipore). The concentration of picric acid was measured with a Unico UV-2100 (USA) variable-wavelength ultraviolet-visible spectrophotometer at 340 nm. Scanning electron microscope (SEM) measurements were taken using an KYKY-EM3200 model. Fourier-transform infrared spectroscopy (FT-IR) spectrum was recorded using KBr tablets on a Thermo Nicolet Nexus 870 FTIR spectrometer (USA). The ultrasonic irradiation was carried out with an Elmasonic S 60 H (ELMA Ultrasonic, Germany) with a constant frequency of 37 kHz.

2.2. Batch sorption experiments

To study the effects of pH on the sorption of picric acid, 30 mg of MWCNT-COOH were dispersed into 15 mL solutions containing a picric acid concentration of 100 mg/L. The initial pH values were adjusted from 1.0 to 10.0 using nitric acid and NaOH at 25±1°C. The amounts of sorbed picric acid were calculated as the difference between the initial and final concentrations when equilibrium was reached. The results are based on at least three replicate experiments for each pH value. To estimate the sorption capacity, 30 mg of MWCNT-COOH were mixed with 20 mL of picric acid solution (concentration range, 10–100 mg/L). After 120 min, the picric acid concentration in the aqueous solutions was determined by ultraviolet-visible spectroscopy. The removal (%) and sorption capacity q (mg/g) were obtained as follows:

$$\text{Removal}\% = \frac{C_0 - C_e}{C_0} \times 100\% \qquad q_e = \frac{(C_0 - C_e) \times V}{m} \tag{1}$$

, where C_0 and C_e are the initial and final concentrations (mg/L) of the picric acid in the aqueous solution, respectively; V (L) is the volume of the picric acid solution, and m (g) is the weight of the sorbent. The kinetic data were analyzed using four kinetic models to gain an understanding of the sorption process. The kinetic experiment was carried out under normal atmospheric conditions at 25±1°C. Initially, 30 mg of MWCNTs were contacted with a 10 mL solution containing a picric acid concentration of 100 mg/L in glass vials, and then, it was stirred for different times with both stirring and ultrasound methods. The adsorbent and solution were separated at predetermined time intervals, filtered using a 0.45 μm membrane filter and analyzed for residual picric acid concentrations as described above.

2.3. Non-linear regression analysis

The adsorption equilibrium data for picric acid on MWCNT-COOH were analyzed by non-linear curve fitting analysis using the MATLAB® software (MathWorks, USA) to fit the three-parameter, four-parameter, and five-parameter isotherm models. The optimization procedure requires an error function to be defined in order to be able to evaluate the fit of the equation to the experimental data [30]. Apart from the correlation coefficient (R^2), the chi-square (χ^2) test and the average relative errors (ARE) were also used to measure the goodness-of-fit [30]. The chi-square test and ARE can be defined as follows:

$$\chi^2 = \sum_{i=1}^{n} \frac{(q_{e,ex} - q_{e,cal})^2}{q_{e,cal}} \qquad ARE = \frac{100}{N} \sum_{i=1}^{n} \left| \frac{(q_{e,ex} - q_{e,cal})}{q_{e,ex}} \right| \tag{2}$$

, where $q_{e,ex}$ and $q_{e,cal}$ are the experimental and calculated values, respectively, and n is the number of measurements. The smaller chi-square and ARE values indicate a better curve fitting.

3. Results and discussion

3.1. Characterization of adsorbent

A SEM image was used to study the morphology of the MWCNT-COOH. Fig. 1a shows that the MWCNTs are curved, rope-like and highly tangled and agglomerated with each other. In addition, the obtained diameters of the MWCNTs were about 30–60 nm.

Fig. 1b shows the FT-IR spectrum of the MWCNT-COOH. The peaks at around 1400–1570 and 3100–3400 cm^{-1} are assigned to the C=C and OH stretching modes, respectively. In addition, the appearance of the absorption peaks at 1703 (C=O) and 1066 (C-O) cm^{-1} clearly shows the carboxylic groups on the MWCNTs. Additionally, the bands at around 2800–2900 could be related to the C-H stretch vibration of the MWCNTs defects.

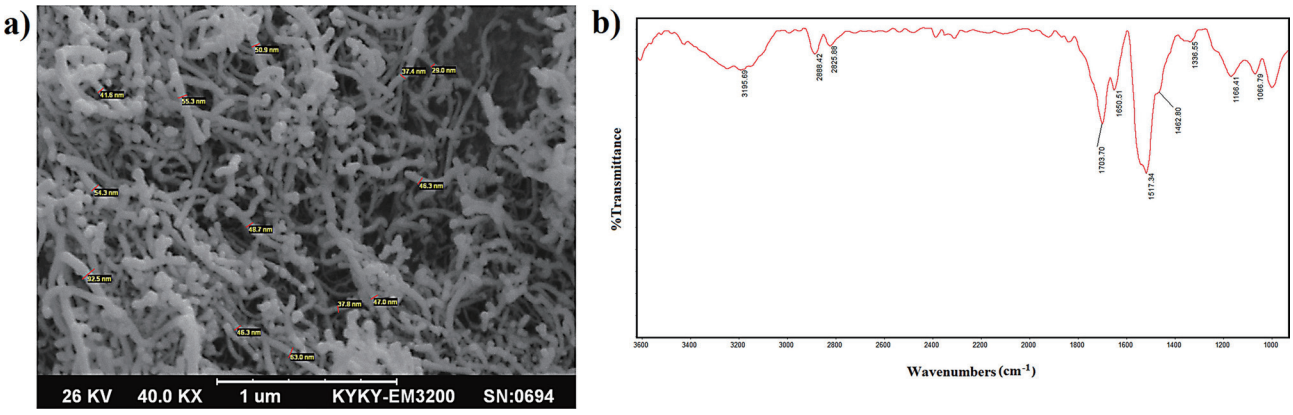

Fig. 1. (a) Scanning electron microscope image of the carboxylated multi-wall carbon nanotube (MWCNT-COOH). (b) Fourier-transform infrared spectrum (after baseline correction) of the MWCNTs-COOH.

3.2. Effect of contact time

The removal percentage of picric acid by MWCNTs was studied as a function of the stirring and ultrasound times shown in Fig. 2. At up to 40 min for the stirring method and 50 min for the ultrasonic method for the initial contact time, the adsorption rate of picric acid on the MWCNT-COOH was relatively rapid and then reached equilibrium at nearly 50 min for the stirring method and at 60 min for the ultrasound method. The fast initial removal indicates a high interaction of the treated sorbent with the picric acid. The final value of the removal percentage of picric acid for the stirring method was 83.2% and 57.1% for the ultrasound method. These values indicate that the adsorption capacity of the CNTs for the stirring method is better than that of the ultrasound method. These differences could be related to the desorption process during the longer sonication time. In fact, ultrasound promotes desorption of adsorbed species from the CNTs, and it is promoted by the collapse of bubbles if it occurs in the vicinity of the sorbent surface.

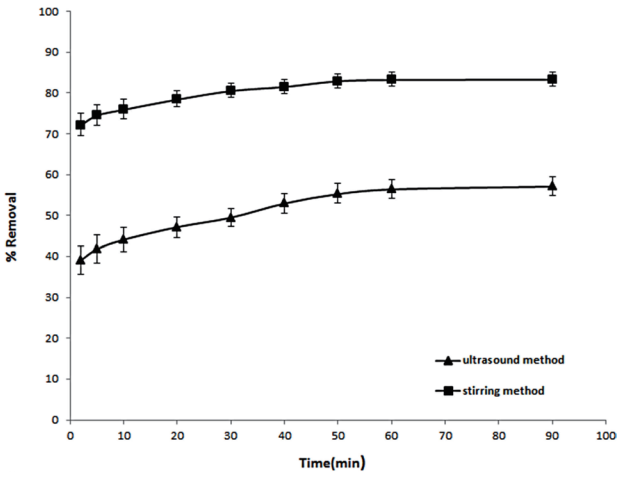

Fig. 2. Effect of the contact time on the adsorption of picric acid from aqueous solutions by the MWCNTs-COOH (experimental conditions, pH=7; mass of MWCNTs, 30 mg/10 mL; picric acid concentration, 100 mg/L).

3.3. Effect of the CNT dosage

Dosage studies were carried out to determine the adsorption percentage of picric acid from aqueous solutions at a picric acid concentration of 100 mg/L. According to Fig. 3, the experimental results revealed that the adsorption percentage of picric acid increased as the MWCNT dosage was increased for both methods. For example, the removal of picric acid was significantly enhanced from 20.3% to 96.29% by the MWCNT-COOH for stirring method and from 14.3% to 87.7% for the ultrasound method when the CNT dosage was increased from 0.01 to 0.07 g. This increase could be related to the greater surface area or more adsorption sites in the high dosage of the MWCNT-COOH. In other words, these values are noticeable for MWCNT-COOH which could be related to the presence of many accessible sites (external surface sorption) on the MWCNT-COOH surface which agrees with the fast transfer of the picric acid species to the surface of the CNTs.

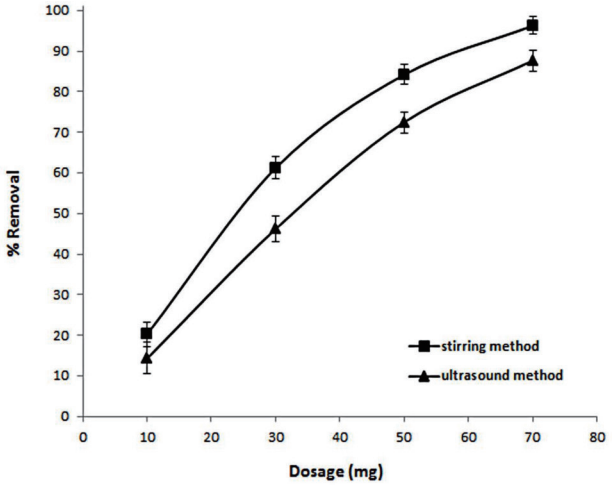

Fig. 3. Effect of the multi-wall carbon nanotube dosage on the adsorption of picric acid from aqueous solution (experimental conditions, pH=7; picric acid concentration, 100 mg/L; volume, 15 mL; contact time, 120 min).

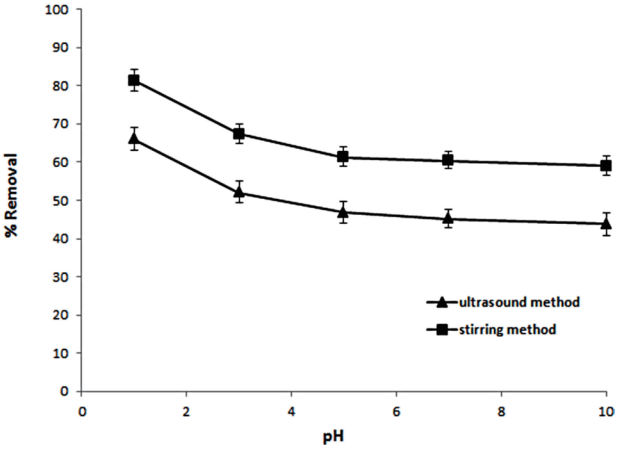

Fig. 4. Effect of pH on the picric acid sorption onto the carboxylated multi-wall carbon nanotube.

3.4. Effect of pH

The effect of pH on the uptake of picric acid is shown in Fig. 4. Because adsorption studies on drinking water purification were more significant at a neutral pH, in this study, we calculated the adsorbed amount of picric acid after equilibrium at C_0=100 mg/L in a pH range between 1.0 and 10.0 for the purpose of comparison. In liquid-phase adsorption, the adsorption capacity of CNTs for aromatic compounds depends on a number of factors such as the physical nature of the adsorbent (pore structure, purity and functional groups), the nature of the adsorbate (its solubility, the presence of functional groups, polarity, molecular weight and size) and the solution conditions such as pH. The experimental results for adsorption in various pHs suggested that there is an increase in the uptake of picric acid at a pH lower than 5. This result could be related to the solubility of picric acid in aqueous solutions. In fact, the solubility of picric acid is dependent on the pH values. In other words, the solubility of picric acid diminishes as the pH value or H^+ concentration decreases or increases, respectively, because the adsorption of phenolic compounds on activated carbon is inversely proportional to the solubility [31]. Therefore, the adsorption percentage of picric acid by the MWCNTs increased as the pH value was decreased. On the other hand, the picric acid dissociates to picrate anion at the higher pH values in which the surface functional groups are either neutral or negatively charged. In these conditions, the electrostatic repulsion between the identical charges decreases the adsorption capacities. In addition, because picrate anions are more soluble in aqueous solution, the stronger adsorbate-water bonds must be broken before adsorption can occur [18,32].

3.5. Kinetic studies

Four kinetic models, the pseudo-first-order, pseudo-second-order, Weber-Morris intra-particle diffusion and Elovich models were used to investigate the rate of the adsorption process and rate controlling step. The best-fit model was selected based on the correlation coefficient values (R^2) of the linear regression.

The pseudo-first-order equation, which was proposed by Lagergren [33], has been used for reversible reactions with an equilibrium being established between liquid and solid phases. This equation is expressed as follows:

$$\log(q_e - q_t) = \log(q_e) - \frac{k_1}{2.303}t \quad (3)$$

, where k_1 is the rate constant of the adsorption (min^{-1}); q_e is the amount adsorbed (mg/g) at equilibrium, and q_t is the amount adsorbed (mg/g) at time t. The plot of log (q_e–q_t) against t gives a linear relationship from which k_1 and q_e are determined from the slope and intercept of the plot, respectively. The pseudo-second-order model can be expressed as given in linear form [15,18]:

$$\frac{t}{q_t} = \frac{1}{k_2 q_e^2} + \frac{1}{q_e}t \quad (4)$$

, where k_2 is the pseudo second-order rate constant of the adsorption (g/mg min), and the other terms have already been defined. The values of q_e and k_2 can be estimated from the slope and intercept of the plot of t/q_t versus t.

Elovich's equation [34] assumes that the solid surfaces of an adsorbent are energetically heterogeneous, and there are no desorption and interactions between the adsorbed species at a low surface coverage. This model can be expressed in linear form as follows:

$$q_t = \frac{1}{b}\ln(ab) + \frac{1}{b}\ln(t) \quad (5)$$

Here, parameter a in the equation is the initial sorption rate (mg g^{-1} min^{-1}), while parameter b is related to the extent of the surface coverage and the activation energy for chemisorption (g mg^{-1}). If this equation applies, it should lead to a straight line for which the a and b coefficients can be calculated from the plot of q_t versus ln t.

The adsorption parameters derived from the application of the pseudo-first-order equation (K_1 and q_e), the pseudo-second-order equation (K_2, q_e) and Elovich's equation (a and b) were calculated and are listed in Table 1. In addition, all plots of the adsorption kinetics are presented in the Supplementary information. The low correlation coefficients, R^2, of the pseudo-first-order and Elovich models for both methods suggest that both models are not applicable to fit the experimental data. In addition, there is no agreement between the $q_{e,exp}$ experimental and q_e calculated values for the pseudo-first-order model (Table 1). The correlation coefficients of the pseudo-second-order model for the stirring and ultrasound methods were 0.9998 and 0.9975, respectively, which indicate the suitability of the pseudo-second-order equation for the MWCNT-COOH for both methods. In addition, the adsorbed values of picric acid at equilibrium (q_e) for the stirring and ultrasound methods were 28.01 and 19.53 mg g^{-1}, respectively, which were near to those from the experimental data. These results show that the sorption of picric acid from an aqueous solution onto MWCNT-COOH with both methods obeys the pseudo-second-order kinetic model and could be used to determine the equilibrium sorption capacity, rate

Table 1. Parameters of the pseudo-first-order, pseudo-second-order, Elovich and intra-particle diffusion models for picric acid sorption onto the MWCNTs-COOH

Methods	Pseudo-first-order model			Pseudo-second-order model			Intra-particle diffusion model		Elovich model			
	k_1 (min^{-1})	q_e (mg/g)	R^2	K_2 (g mg^{-1} min^{-1})	q_e (mg/g)	R^2	K_{id} (mg g^{-1} $min^{-0.5}$)	R^2	a	b	R^2	q_{ex}
Stirring	0.0767	5.86	0.9184	0.0392	28.01	0.9998	0.4969	0.9307	1.9×10^9	0.9214	0.9777	27.76
Ultrasound	0.0516	7.92	0.9402	0.0162	19.53	0.9975	0.8109	0.9667	1206.15	0.5831	0.9518	19.03

Temperature, 298 K; initial picric acid concentration, 100 mg L^{-1}; mass of MWCNTs, 30 mg; volume of solution, 10 mL; and pH of the sample solution, 7.0.
MWCNTs-COOH, carboxylated multi-wall carbon nanotube.

constants, and percentage of picric acid removal.

In order to better understand the adsorption mechanism that affects the kinetics of adsorption, the kinetic data were fitted to the Weber-Morris intra-particle diffusion model [15,35]. In fact, it is described by external mass transfer and intra-particle diffusion. This model is expressed as follows:

$$q_t = k_{id}t^{0.5} + C_i \quad (6)$$

, where k_{id} (mole $g^{-1}min^{1/2}$) is the rate constant of the intra-particle diffusion, and C_i is proportional to the boundary layer thickness. If the regression of q_t versus $t^{1/2}$ gives a straight line, then intra-particle diffusion is involved in the adsorption process, and if this line passes through the origin, then intraparticle diffusion is the sole rate-limiting step, and the k_{id} can be calculated from the slope and C_i from the intercept. The intra-particle kinetic model of picric acid sorption by MWCNT-COOH for both methods is shown in Fig. 5. The nonzero intercepts of the plots in each case were a clear indication that intra-particle diffusion is not the rate-limiting step of the sorption mechanism. Hence, the intra-particle diffusion model is not the only rate-controlling step. The difference in the rate of mass transfer during the initial and final stages of adsorption could cause the deviation in the straight lines from the origin. According to Fig. 5, it is clear that intra-particle diffusion of picric acid within the MWCNT-COOH with both methods occurred in two stages because the plots contain two different straight lines. The initial adsorption stage is approximately rapid for the MWCNT-COOH for both methods. It is from 0 to 50 min for the stirring method and from 0 to 60 min for the ultrasound method, which is due to the fast diffusion of the picric acid from the aqueous phase to the outer-surface of the MWCNTs. The second stage is a slow adsorption and is from 50 to 90 min for the stirring method and from 60 to 90 min for the ultrasound method which could be attributed to the intra-particle diffusion of the picric acid molecules into the porous structure of the MWCNT-COOH. In other words, when the adsorption on the exterior surface became saturated, the picric acid molecules entered into the pores of the adsorbent and were adsorbed by the interior surface of the mesopores. Thus, these results confirm that both external surface sorption and intra-particle diffusion participate in the process of picric acid adsorption by MWCNTs and that the intra-particle diffusion model is not the only rate-controlling step. The results are shown in Table 1.

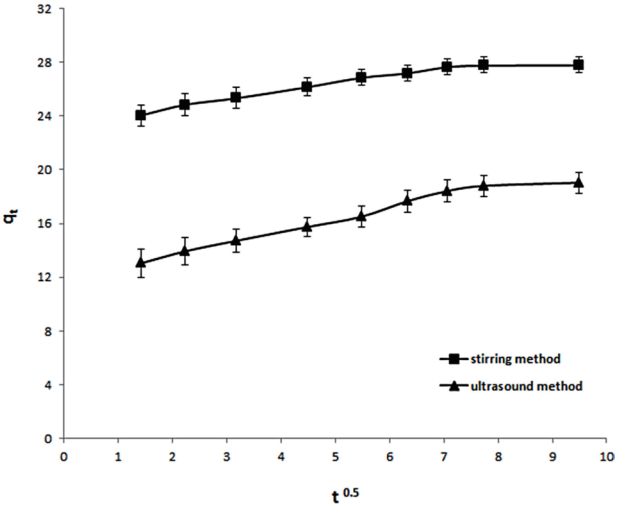

Fig. 5. Linearized intra-particle diffusion kinetic model of the picric acid sorption onto the multi-wall carbon nanotubes.

3.6. Adsorption isotherms

Adsorption isotherms are the mathematical equations in which the ratio between the adsorbate concentrations in the solid phase and that in the liquid phase at a constant temperature and pH is studied. In fact, it indicates how a substance from aqueous media transfers to a solid phase when an equilibrium state is established in a system. In this study, the two-parameter (Langmuir, Freundlich, Halsey, Tempkin, Harkins-Jura, Fowler-Guggenheim), three-parameters (Redlich-Peterson, Khan, Radke-Prausnitz, Toth), four-parameters (Fritz-Schlunder and Baudu) and five-parameter (Fritz-Schlunder) isotherm models along with their constant values, which describe the surface properties and affinity of the adsorbent, were used to express the mechanism of adsorption. All plots of the adsorption isotherms are presented in Supplementary data.

3.6.1. Two-parameter isotherms

3.6.1.1. Langmuir isotherm

The Langmuir model [30,36] assumes that the maximum sorption capacity corresponds to a complete monolayer coverage of the molecules on the adsorbent surface with no

Table 2. The parameters of the different isotherm models for picric acid removal from aqueous solutions by the MWCNT-COOH

Methods	Isotherm models	The calculated parameters			
Stirring Ultrasound	Langmuir (type 1)	q_m (mg/g)	B (L/mg)	R^2	Plot
	$\frac{C_e}{q_e} = \frac{1}{bq_m} + \frac{C_e}{q_m}$	28.49	0.531	0.999	$\frac{c_e}{q_e}$ vs. C_e
		22.03	0.2722	0.9971	
Stirring Ultrasound	Langmuir (type 2)				
	$\frac{1}{q_e} = \frac{1}{q_m} + \frac{1}{bq_mC_e}$	26.52	1.036	0.9973	$\frac{1}{q_e}$ vs. $\frac{1}{c_e}$
		20.45	0.449	0.9929	
Stirring Ultrasound	Langmuir (type 3)				
	$q_e = q_m - \frac{q_e}{bC_e}$	26.91	0.9870	0.9713	q_e vs. $\frac{q_e}{c_e}$
		20.799	0.4253	0.9512	
Stirring Ultrasound	Langmuir (type 4)				
	$\frac{q_e}{C_e} = bq_m - bq_e$	27.065	0.9586	0.9713	$\frac{q_e}{c_e}$ vs. q_e
		21.005	0.4045	0.9512	
Stirring Ultrasound	Freundlich	K_f (mg/g) $(mg/L)^n$	**n**	**R^2**	ln q_e vs. ln C_e
	$\ln q_e = \ln K_f + \frac{1}{n}\ln C_e$	10.604	3.77	0.9133	
		6.79	3.45	0.9537	
Stirring Ultrasound	**Halsey**	**K_H**	**n_H**	**R^2**	ln q_e vs. ln $1/C_e$
	$\ln q_e = \frac{1}{n_H}\ln K_H - \frac{1}{n_H}\ln\frac{1}{C_e}$	7432.01	3.77	0.9133	
		739.06	3.45	0.9537	
Stirring Ultrasound	**Tempkin**	**K_1(L/g)**	**K_2**	**R^2**	q_e vs. ln C_e
	$q_e = K_1 \ln K_2 + K_1 \ln C_e$	4.0117	21.92	0.982	
		3.5456	6.55	0.9865	
Stirring Ultrasound	**Harkins-Jura**	**A_{HJ}**	**B_{HJ}**	**R^2**	$1/q_e^2$ vs. log C_e
	$\frac{1}{q_e^2} = \frac{B_{HJ}}{A_{HJ}} - \frac{1}{A_{HJ}}\log C_e$	111.11	1.611	0.7624	
		76.92	1.784	0.8479	
Stirring Ultrasound	**Fowler–Guggenheim**	**W (kJ/mol)**	**K_{FG}**	**R^2**	$\ln\frac{C_e(1-\theta)}{\theta}$ vs. θ
	$\ln\frac{C_e(1-\theta)}{\theta} = -\ln K_{FG} + \frac{2W\theta}{RT}$	-14.102	0.0000843	0.9791	
		-11.574	0.0003456	0.9984	

interaction between the sorbed molecules. In addition, this empirical model refers to the same activation energy of adsorption when the adsorption of each molecule occurs at definite localized sites onto a homogeneous surface without transmigration of the adsorbate in the plane of the surface. The Langmuir equation in non-linearized form can be written as follows:

$$q_e = \frac{bq_mC_e}{1 + bC_e} \quad (7)$$

, where q_e (mg g^{-1}) and C_e (mg L^{-1}) are the amount of solute adsorbed per unit weight of adsorbent at equilibrium and the picric acid concentration at equilibrium, respectively. q_m (mg g^{-1}) is the maximum adsorption capacity, and b is the adsorption equilibrium constant (L mg^{-1}) that is related to the free energy of adsorption. The four linear forms of the Langmuir isotherm with its parameters are shown in Table 2. Among the four forms, the values for the obtained regression coefficients from the Type-1 and Type-2 equations for both methods indicate that the adsorption of picric acid on the MWCNTs follows the Langmuir isotherm. In other words, Type 1-2 equations are the best form for the interpretation of experimental data, which had the highest coefficient of correlation for the MWCNTs with the stirring and ultrasound methods compared to the other forms. In addition, the obtained Langmuir parameters (b and q_m) from the four linear models were different.

Table 3. The calculated R_L values of the Langmuir isotherm at concentrations of 10-100 mg/L for both methods

C_0 (mg/L)	Langmuir models	The calculated R_L values	
		Stirring method	Ultrasound method
10	Type 1	0.158479	0.268673
30		0.059067	0.109099
50		0.036298	0.068446
70		0.026199	0.049865
90		0.020496	0.039219
100		0.018484	0.035436
10	Type 2	0.088028	0.182149
30		0.031172	0.069109
50		0.018939	0.042644
70		0.013602	0.030836
90		0.010611	0.024149
100		0.00956	0.021786
10	Type 3	0.091996	0.190367
30		0.032669	0.07268
50		0.019861	0.044914
70		0.014267	0.032498
90		0.011132	0.02546
100		0.01003	0.022973
10	Type 4	0.094464	0.198216
30		0.033604	0.076132
50		0.020437	0.047114
70		0.014684	0.034112
90		0.011458	0.026734
100		0.010324	0.024125

It could be related to the transformations of the non-linear model to the linear forms which cause a change in the error structure of the standard least-squares method. Additionally, the dimensionless equilibrium parameter or separation factor, R_L, is the essential characteristics of the Langmuir isotherm as follows [16,15]:

$$R_L = \frac{1}{1 + bC_0} \tag{8}$$

, where b is the Langmuir constant, and C_0 is the initial concentration of adsorbate in solution. These values show the type of isotherm to be irreversible (R_L=0), favorable (0<R_L<1), linear (R_L=1) or unfavorable (R_L>1). The calculated values of R_L for both methods are shown in Table 3. From Table 3, the R_L values of the Type 1 and 2 models were found to be around 0.0096–0.1585 for the stirring method and 0.02179–0.2687 for the ultrasound method indicating a favorable behavior toward picric acid adsorption.

3.6.1.2. Freundlich and Halsey isotherms

The Freundlich [37] and Halsey [18,38] isotherms can be used for multilayer adsorption and heterogeneous surfaces with non-uniform distribution of adsorption heat. The linearized form of the Freundlich equation is as follows:

$$\ln q_e = \ln K_f + \frac{1}{n} \ln C_e \tag{9}$$

, where K_F is an empirical constant related to the sorption capacity of the adsorbent (L mg^{-1})(L $g^{-1})^{1/n}$, and constant *n* is a constant indicative of the intensity of the adsorption and varies with the surface heterogeneity and affinity. The values of k_f and *n* can be calculated by plotting ln q_e versus ln C_e. Moreover, the Halsey equation can be given as follows:

$$\ln q_e = \frac{1}{n_H} \ln K_H - \frac{1}{n_H} \ln \frac{1}{C_e} \tag{10}$$

, where K_H and n_H are the Halsey constants, which can be obtained from the slope and intercept of the linear plot based on $\ln(q_e)$ versus $\ln 1/C_e$, respectively. The related Freundlich and Halsey isotherm parameters were calculated and then tabulated in Table 2. The low correlation coefficients of the Freundlich and Halsey models for the stirring (0.9133) and ultrasound (0.9537) methods show that they are not suitable for the interpretation of the experimental data. In other words, these models could not interpret the data reasonably well for the adsorption of picric acid onto the MWCNT-COOH with both methods. Then, the assumption of multilayer adsorption by the Freundlich and Halsey models is not in agreement with the experiment in the studied concentration range.

3.6.1.3. Tempkin isotherm

Tempkin [39] suggested that due to adsorbent-adsorbate interactions, the heat of adsorption of all molecules linearly decrease with the surface coverage. In addition, it assumes that the adsorption is characterized by a uniform distribution of the binding energies up to some maximum binding energy. The linearized form of the Tempkin model has generally been applied in the following form:

$$q_e = K_1 \ln K_2 + K_1 \ln C_e \tag{11}$$

, where k_1 is related to the heat of adsorption (L/g), and K_2 is the dimensionless Tempkin isotherm constant. The Tempkin parameters (k_1 and k_2) can be determined from the linear plots of q_e and ln C_e. As can be seen in Table 2, the values for the regression coefficients for the stirring and ultrasound methods were 0.982 and 0.9865, respectively, which relatively show good agreement with the picric acid adsorption on the MWCNT-COOH.

3.6.1.4. Harkins-Jura isotherm

The Harkin-Jura model assumes the existence of a heterogeneous pore distribution in the surface of adsorbents and can be

applied to multi-layer adsorptions [40]. This model is written as follows:

$$\frac{1}{q_e^2} = \frac{B_{HJ}}{A_{HJ}} - \frac{1}{A_{HJ}} \log C_e \quad (12)$$

Here, the Harkins-Jura isotherm parameters, A_{HJ} and $B_{HJ,}$ can be obtained from the linear plot of $1/q_e^2$ against log C_e. The values of the Harkins-Jura constants together with the regression coefficients are presented in Table 2 for the adsorption of picric acid onto MWCNT-COOH for both methods. The low regression coefficients of the MWCNTs-COOH for both methods show the inapplicability of this model for picric acid adsorption onto MWCNTs.

3.6.1.5. Fowler-Guggenheim isotherm

The Fowler-Guggenheim isotherm [41] describes the presence of lateral interactions between adsorbed molecules on MWCNTs. The linearized form of this model can be given as follows:

$$\ln \frac{C_e(1-\theta)}{\theta} = -\ln K_{FG} + \frac{2W\theta}{RT} \quad (13)$$

, where K_{FG} is the Fowler-Guggenheim equilibrium constant (L mg^{-1}); $\theta=(1-C_e/C_0)$ is the degree of surface coverage; W is the interaction energy between adsorbed molecules (kJ mol^{-1}); R is the universal gas constant and is equal to 8.314 J mol^{-1} K^{-1}, and T is the absolute temperature (K). The W sign determines the interactions between the adsorbed molecules. Therefore, if W is positive, the interaction between the adsorbed molecules is attractive and the heat of adsorption due to the increased interaction between the adsorbed molecules increases with the loading of adsorbates. Additionally, if W is negative, the heat of adsorption decreases with the loading of adsorbates, and hence, the interaction among the adsorbed molecules is repulsive. When there is no interaction between adsorbed molecules, W=0. The values of K_{FG} and W were evaluated from the intercept and the slope, respectively, of the linear plot of ln $C_e(1-\theta)/\theta$ versus θ based on the experimental data. The adsorption data for the picric acid adsorption onto the MWCNT-COOH for both methods were calculated and summarized in Table 2. As can be seen in Table 2, the negative values of the interaction energy (W) for both methods indicate the presence of repulsion between the adsorbed molecules, and the regression coefficients of the MWCNTs-COOH for both methods were relatively good.

3.6.2. Isotherm models of more than two parameters

Generally, the parameters of isotherm models have been frequently obtained by linear regression. However, modifying the non-linear isotherm equations to linear forms violate the theories existing behind the model which can cause an estimation error. Hence, nonlinear regression is a more useful method to estimate the parameters of the model and that the calculated parameters with this method are more relevant than those obtained with linear regression. In addition, nonlinear regression can be applied to the isotherm model which cannot be linearized. Therefore, nonlinear regression was used for the isotherm models with more than two parameters. Table 4 presents the calculated parameters of the adsorption isotherms and their characterizations obtained using the non-linear fitting analysis. As can be seen from Table 4, the coefficients of correlation for all the models are very good (≥0.9921). Thus, the values of the chi-square test and the ARE will determine the better model. Among the three-parameter isotherms, the best representation of the experimental results for the adsorption was obtained with the Redlich-Peterson model for the ultrasound method because it has the minimum ARE and chi-square values and maximum regression coefficients. The characterization of the Redlich-Peterson model is presented in Table 4. This model reduces to the Langmuir equation when its heterogeneity parameter is g=1. The obtained g values for both methods were close to unity (0.9245 and 0.901) which shows the adsorption tends to be a Langmuir behavior. In other words, the adsorption process is achieved by a homogeneous surface in a monolayer distribution.

The Khan model presents a better adjustment for the interpretation of the obtained data from the stirring method. The maximum uptake values (q_s) were well predicted by the model with high correlation coefficients and minimum ARE and chi-square values. Of course, this model shows that the maximum adsorption capacities are lower than those of the Langmuir model for both methods; however, the difference in the maximum adsorption capacities between the two methods was similar to those of the Langmuir model. The Radke-Prausnitz and Toth models have remarkable similarity in accuracy and fitness with the Redlich-Peterson and Khan models, respectively. The adsorption data of the four-parameter isotherm models of Fritz-Schlunder and Baudu are presented in Table 4. The obtained data from the Fritz-Schlunder model were similar to the Redlich-Peterson one for the stirring method which shows the characterization of the Langmuir model. However, for the ultrasound method, despite the high regression coefficients (0.997) and low ARE and chi-squire values, this model cannot describe the experimental equilibrium data. The Baudu model provides an excellent description of the experimental results. The maximum adsorption capacities for both methods are slightly higher than those calculated by the Langmuir model which shows good agreement with this model. The adsorption data of the five-parameter isotherm model of Fritz-Schlunder were analyzed and presented in Table 4. From Table 4, the coefficients of correlation for both methods are very good (≥0.997), and the ARE and chi-square values for picric acid are relatively low. The values for the maximum adsorption capacity obtained with the Fritz-Schlunder equation were similar to those calculated by the Khan model. Comparing the three-parameter, four-parameter, and five-parameter models, it seems that Baudu is the most logical model for fitting the adsorption isotherms of both methods because the q_m is close to the experimental values. In addition, the fitting degree of the three-parameter isotherms for the stirring and ultrasound methods was as follows: Khan > Toth > Radke-Prausnitz > Redlich-Peterson, and Redlich-Peterson > Radke-Prausnitz > Toth >Khan, respectively.

DOI: http://dx.doi.org/10.5714/CL.2017.22.014

Table 4. The calculated parameters of the isotherm models of more than two parameters for picric acid removal from aqueous solutions by MWCNT-COOH.

Methods	Isotherm models	The calculated parameters							Characterization	Ref
	Redlich-Peterson	k_R	a_R	**g**	$\mathbf{R^2}$	χ^2	%ARE		It is a hybrid isotherm featuring both Langmuir and Freundlich isotherms. The model can be applied either in homogeneous or heterogeneous systems due to its versatility. In addition, it approaches the Freundlich isotherm at a high concentration and is in accordance with the low concentration limit of the Langmuir equation. *g* is the exponent which lies between 0 and 1.	[42]
Stirring	$q_e = \frac{k_R C_e}{1 + a_R C_e^g}$	32.82	1.58	0.9245	0.9992	0.01515	0.3221			
Ultrasound		10.87	0.7556	0.901	0.9925	0.06663	0.1519			
	Khan	$\mathbf{q_S}$	$\mathbf{a_K}$	$\mathbf{b_K}$	$\mathbf{R^2}$	χ^2	%ARE		It is a generalized model for the pure solutions. At relatively high correlation coefficients and minimum chi-square values, the maximum uptake values were well predicted. q_s: the maximum uptake values; b_K: the model constant; a_K: the Khan model exponent. Adsorption data of this model is reported for phenol and phenol derivatives in aqueous medium for single and bisolute systems.	[43]
Stirring	$q_e = \frac{q_s b_K C_e}{(1 + b_K C_e)^{a_K}}$	19.14	0.9151	1.608	0.9992	0.00947	0.2492			
Ultrasound		13.97	0.8876	0.7152	0.9921	0.07168	0.1802			
	Radke-Prausnitz	$\mathbf{a_{RP}}$	$\mathbf{r_R}$	$\mathbf{\beta_R}$	$\mathbf{R^2}$	χ^2	%ARE		It is used in the adsorption of organic solutes from dilute aqueous solutions. The correlation of this model is usually predicted well by the low chi-square values. a_{RP}: maximum adsorption capacities; r_R: the equilibrium constant; β_R: the model exponent of Radke-Prausnitz.	[44]
Stirring	$q_e = \frac{a_{RP} r_R C_e^{\beta_R}}{1 + r_R C_e^{\beta_{R-1}}}$	32.82	0.6328	0.07551	0.9992	0.01515	0.3072			
Ultrasound		10.87	1.323	0.09901	0.9925	0.06666	0.1781			
	Toth	$\mathbf{k_T}$	$\mathbf{a_T}$	**t**	$\mathbf{R^2}$	χ^2	%ARE		This model improved the Langmuir isotherm fittings and is useful in describing the sorption in heterogeneous systems such as phenolic compounds on carbon. k_T and a_T are the model constant; t: the Toth model exponent.	[45]
Stirring	$q_e = \frac{k_T C_e}{(a_T + C_e)^{1/t}}$	19.92	0.6218	1.093	0.9995	0.00947	0.2638			
Ultrasound		13.46	1.398	1.127	0.9921	0.07168	0.0379			
	Fritz-Schlunder	**A**	**B**	**α**	**β**	$\mathbf{R^2}$	χ^2	**%ARE**	This model is the modified four-parameter equation of the Langmuir-Freundlich type. *A* and *B* are the Fritz-Schlunder parameters, and α and β are the Fritz-Schlunder equation exponents. When $\alpha = \beta = 1$, it reduces to the Langmuir equation.	[46]
Stirring	$q_e = \frac{A C_e^{\alpha}}{1 + B C_e^{\beta}}$	32.82	1.58	1	0.9245	0.9992	0.01515	0.3221		
Ultrasound	with α and $\beta \leq 1$	6.633	0.0614	0.496	0.7728	0.997	0.04791	0.3758		
	Baudu	$\mathbf{q_m}$	**b**	**x**	**y**	$\mathbf{R^2}$	χ^2	**%ARE**	This equation shows that the calculation of the Langmuir coefficients at different equilibrium concentrations is not constant in a broad concentration range. q_e is the adsorbed amount at equilibrium (mg g^{-1}), C_e the equilibrium concentration of the adsorbate (mg L^{-1}), q_m the Baudu maximum adsorption capacity (mg g^{-1}), *b* the equilibrium constant, and *x* and *y* the Baudu parameters.	[47]
Stirring	$q_e = \frac{q_m b C_e^{(1+x+y)}}{1 + b C_e^{(1+x)}}$	29.37	0.7121	-0.2599	-9.94×10^{-11}	0.9957	0.07525	0.5205		
Ultrasound	with $(1 + x + y)$ and $(1 + x) < 1$	24.63	0.3351	-0.283	-0.007	0.9956	0.05356	0.5567		
	Fritz-Schlunder	$\mathbf{q_m}$	$\mathbf{K_1}$	$\mathbf{K_2}$	$\mathbf{m_1}$	$\mathbf{m_2}$	$\mathbf{R^2}$	χ^2	**%ARE**	This model is reduced to the Langmuir model when the exponents m_1 and m_2 are equal to unity. For higher liquid-phase concentrations, the model of Fritz-Schlunder is converted to the Freundlich model. q_e is the adsorbed amount at equilibrium (mg g^{-1}), C_e the equilibrium concentration of the adsorbate (mg L^{-1}), q_m the Fritz-Schlunder maximum adsorption capacity (mg g^{-1}) and K_1, K_2, m_1, and m_2 the Fritz-Schlunder parameters.	[46]
Stirring	$q_e = \frac{q_m K_1 C_e^{m_1}}{1 + K_2 C_e^{m_2}}$	18.31	1.792	1.58	1	0.9245	0.9992	0.01512	0.2962		
Ultrasound	with m_1 and $m_2 \leq 1$	11.48	0.5779	0.0614	0.496	0.7728	0.997	0.04770	0.3564		

ARE, average relative errors.

4. Conclusions

The study showed that MWCNT-COOH has the ideal performance for the adsorption of picric acid. The results showed that MWCNT-COOH has a higher sorption capacity for the stirring method relative to that for the ultrasound method. The sorption kinetics of picric acid by MWCNT-COOH was found to follow the pseudo-second-order model for both methods. Among the two-parameter models, the Langmuir model better described the isotherm data. In the case of more than two parameters, the Baudu model was found to provide the closest fit to the equilibrium experimental data with a high R^2 and relatively low ARE and chi-square values. In addition, the W values of both methods for MWCNTs were negative, which show the presence of the repulsion among the adsorbed molecules

Conflict of Interest

No potential conflict of interest relevant to this article was reported.

Acknowledgements

I would like to thank Dr. Mehrdad Khanpour for the helpful discussions as well as the Research Vice Presidency of the Ayatollah Amoli branch, Islamic Azad University for their encouragement and financial support.

References

[1] Rappoport Z. The Chemistry of Phenols, John Wiley & Sons, Chichester (2003).

[2] Aggarwal P, Misra K, Kapoor SK, Bhalla AK, Bansal RC. Effect of surface oxygen complexes of activated carbon on the adsorption of 2,4,6-trinitrophenol. Def Sci J, **48**, 219 (1998). https://doi.org/10.14429/dsj.48.3902.

[3] Boileau J, Fauquigonon C, Napoly C. Explosives. In: Gerharts W, Tamamoto YS, Kaudy L, Rounsaviille JF, Schulz G, eds. Ullmann's Encyclopedia of Industrial Chemistry, VCH, Weinheim, 145 (1987).

[4] Roth J. Picric Acid. In: Kaye SM, Herman HL, eds. Encyclopedia of Explosives and Related Items, US Army Armament Research and Development Command, Dover, 285 (1980).

[5] US Environmental Protection Agency, Ambient Water Quality Criteria for Nitrophenol, USEPA, Washington DC, (1980).

[6] Nipper M, Carr RS, Biedenbach JM, Hooten RL, Miller K. Fate and effects of picric acid and 2,6-DNT in marine environments: toxicity of degradation products. Mar Pollut Bull, **50**, 1205 (2005). https://doi.org/10.1016/j.marpolbul.2005.04.019.

[7] Kavlock RJ, Oglesby LA, Hall LL, Fisher HL, Copeland F, Logsdon T, Ebron-McCoy M. In vivo and in vitro structure-dosimetry-activity relationships of substituted phenols in developmental toxicity assays. Reprod Toxicol, **5**, 255 (1991). https://doi.org/10.1016/0890-6238(91)90059-o.

[8] World Health Organization, Guidelines for Drinking Water Quality. Vol. II: Health Criteria and Supporting Information, WHO, Geneva, (1984).

[9] US Environmental Protection Agency, Technical Support Document for Water Quality Based Toxics Control, EPA/440/485032, USEPA, Washington, DC (1985).

[10] Shen XE, Shan XQ, Dong DM, Hua XY, Owens G. Kinetics and thermodynamics of sorption of nitroaromatic compounds to as-grown and oxidized multiwalled carbon nanotubes. J Colloid Interface Sci, **330**, 1 (2009). https://doi.org/10.1016/j.jcis.2008.10.023.

[11] Galán J, Rodríguez A, Gómez JM, Allen SJ, Walker GM. Reactive dye adsorption onto a novel mesoporous carbon. Chem Eng J, **219**, 62 (2013). https://doi.org/10.1016/j.cej.2012.12.073.

[12] Goscianska J, Marciniak M, Pietrzak R. Mesoporous carbons modified with lanthanum(III) chloride for methyl orange adsorption. Chem Eng J, **247**, 258 (2014). https://doi.org/10.1016/j.cej.2014.03.012.

[13] Goscianska J, Pietrzak R. Removal of tartrazine from aqueous solution by carbon nanotubes decorated with silver nanoparticles. Catal Today, **249**, 259 (2015). https://doi.org/10.1016/j.cattod.2014.11.017.

[14] Akbarzadeh H, Abbaspour M, Salemi S. Carbon monoxide adsorption on the single-walled carbon nanotube supported gold-silver nanoalloys. New J Chem, **40**, 310 (2016). https://doi.org/10.1039/C5NJ01382H.

[15] Jahangiri M, Kiani F, Tahermansouri H, Rajabalinezhad A. The removal of lead ions from aqueous solutions by modified multi-walled carbon nanotubes with 1-isatin-3-thiosemicarbazone. J Mol Liq, **212**, 219 (2015). https://doi.org/10.1016/j.molliq.2015.09.010.

[16] Tahermansouri H, Ahi RM, Kiani F. Kinetic, equilibrium and isotherm studies of cadmium removal from aqueous solutions by oxidized multi-walled carbon nanotubes and the functionalized ones with thiosemicarbazide and their toxicity investigations: a comparison. J Chin Chem Soc, **61**, 1188 (2014). https://doi.org/10.1002/jccs.201400197.

[17] Wang Y, Gu Z, Yang J, Liao J, Yang Y, Liu N, Tang J. Amidoxime-grafted multiwalled carbon nanotubes by plasma techniques for efficient removal of uranium(VI). Appl Surf Sci, **320**, 10 (2014). https://doi.org/10.1016/j.apsusc.2014.08.182.

[18] Tahermansouri H, Dehghan Z, Kiani F. Phenol adsorption from aqueous solutions by functionalized multiwalled carbon nanotubes with a pyrazoline derivative in the presence of ultrasound. RSC Adv, **5**, 44263 (2015). https://doi.org/10.1039/c5ra02800k.

[19] Strachowski P, Bystrzejewski M. Comparative studies of sorption of phenolic compounds onto carbon-encapsulated iron nanoparticles, carbon nanotubes and activated carbon. Colloids Surf A Physicochem Eng Asp, **467**, 113 (2015). https://doi.org/10.1016/j.colsurfa.2014.11.044.

[20] Ihsanullah I, Asmaly HA, Saleh TA, Laoui T, Gupta VK, Atieh MA. Enhanced adsorption of phenols from liquids by aluminum oxide/carbon nanotubes: comprehensive study from synthesis to surface properties. J Mol Liq, **206**, 176 (2015). https://doi.org/10.1016/j.molliq.2015.02.028.

[21] Atieh MA. Removal of phenol from water different types of carbon: a comparative analysis. APCBEE Procedia, **10**, 136 (2014). https://doi.org/10.1016/j.apcbee.2014.10.031.

[22] Hüffer T, Schroth S, Schmidt TC. Influence of humic acids on sorption of alkanes by carbon nanotubes: implications for the dominant sorption mode. Chemosphere, **119**, 1169 (2015). https://doi.org/10.1016/j.chemosphere.2014.09.097.

[23] Yu F, Sun S, Han S, Zheng J, Ma J. Adsorption removal of ciprofloxacin by multi-walled carbon nanotubes with different oxygen contents from aqueous solutions. Chem Eng J, **285**, 588 (2016). https://doi.org/10.1016/j.cej.2015.10.039.

[24] Ncibi MC, Sillanpää M. Optimized removal of antibiotic drugs from aqueous solutions using single, double and multi-walled carbon nanotubes. J Hazard Mater, **298**, 102 (2015). https://doi.org/10.1016/j.jhazmat.2015.05.025.

[25] Wu W, Yang K, Chen W, Wang W, Zhang J, Lin D, Xing B. Correlation and prediction of adsorption capacity and affinity of aromatic compounds on carbon nanotubes. Water Res, **88**, 492 (2016). https://doi.org/10.1016/j.watres.2015.10.037.

[26] Kim DW, Kim YD, Choi KH, Lim DC, Lee KH. Comparison of the toluene adsorption capacities of various carbon nanostructures. Carbon Lett, **12**, 81 (2011). https://doi.org/10.5714/CL.2011.12.2.081.

[27] Asfaram A, Ghaedi M, Goudarzi A, Rajabi M. Response surface methodology approach for optimization of simultaneous dye and metal ion ultrasound-assisted adsorption onto Mn doped Fe_3O_4-NPs loaded on AC: kinetic and isothermal studies. Dalton Trans, **44**, 14707 (2015). https://doi.org/10.1039/C5DT01504A.

[28] Saghanejhad Tehrani M, Zare-Dorabei R. Highly efficient simultaneous ultrasonic-assisted adsorption of methylene blue and rhodamine B onto metal organic framework MIL-68(Al): central composite design optimization. RSC Adv, **6**, 27416 (2016). https://doi.org/10.1039/C5RA28052D.

[29] Dashamiri S, Ghaedi M, Dashtian K, Rahimi MR, Goudarzi A, Jannesar R. Ultrasonic enhancement of the simultaneous removal of quaternary toxic organic dyes by CuO nanoparticles loaded on activated carbon: central composite design, kinetic and isotherm study. Ultrason Sonochem, **31**, 546 (2016). https://doi.org/10.1016/j.ultsonch.2016.02.008.

[30] Foo KY, Hameed BH. Insights into the modeling of adsorption isotherm systems. Chem Eng J, **156**, 2 (2010). https://doi.org/10.1016/j.cej.2009.09.013.

[31] Daifullah AAM, Girgis BS. Removal of some substituted phenols by activated carbon obtained from agricultural waste. Water Res, **32**, 1169 (1998). https://doi.org/10.1016/S0043-1354(97)00310-2.

[32] Terzyk AP. Further insights into the role of carbon surface functionalities in the mechanism of phenol adsorption. J Colloid Interface Sci, **268**, 301 (2003). https://doi.org/10.1016/S0021-9797(03)00690-8.

[33] Lagergren S. Zur theorie der sogenannten adsorption geloster stoffe, Kungliga Svenska Vetenskapsakademiens. Handlingar, **24**, 1 (1898).

[34] Chien SH, Clayton WR. Application of Elovich equation to the kinetics of phosphate release and sorption in soils. Soil Sci Soc Am J, **44**, 265 (1980). https://doi.org/10.2136/sssaj1980.03615995004400020013x.

[35] Weber WJ, Morris JC. Kinetics of adsorption on carbon from solution. J Sanit Eng Div Am Soc Civ Eng, **89**, 31 (1963).

[36] Langmuir I. The constitution and fundamental properties of solids and liquids: part I. solids. J Am Chem Soc, **38**, 2221 (1916). https://doi.org/10.1021/ja02268a002.

[37] Freundlich HMF. Over the adsorption in solution. J Phys Chem, **57**, 385 (1906).

[38] Halsey GD. The role of surface heterogeneity. Adv Catal, **4**, 259 (1952). https://doi.org/10.1016/S0360-0564(08)60616-1.

[39] Tempkin MI, Pyzhev V. Kinetics of ammonia synthesis on promoted iron catalysis. Acta Physicochimica URSS, **12**, 327 (1940).

[40] Kausar A, Bhatti HN, MacKinnon G. Equilibrium, kinetic and thermodynamic studies on the removal of U(VI) by low cost agricultural waste. Colloids Surf B Biointerfaces, **111**, 124 (2013). https://doi.org/10.1016/j.colsurfb.2013.05.028.

[41] Fowler RH, Guggenheim EA. Statistical Thermodynamics, Cambridge University Press, London, 431 (1939).

[42] Redlich O, Peterson DL. A useful adsorption isotherm. J Phys Chem, **63**, 1024 (1959). https://doi.org/10.1021/j150576a611.

[43] Khan AR, Ataullah R, Al-Haddad A. Equilibrium adsorption studies of some aromatic pollutants from dilute aqueous solutions on activated carbon at different temperatures. J Colloid Interface Sci, **194**, 154 (1997). https://doi.org/10.1006/jcis.1997.5041.

[44] Vijayaraghavan K, Padmesh TVN, Palanivelu K, Velan M. Biosorption of nickel(II) ions onto Sargassum wightii: application of two-parameter and three-parameter isotherm models. J Hazard Mater, **133**, 304 (2006). https://doi.org/10.1016/j.jhazmat.2005.10.016.

[45] Zhang L, Zeng Y, Cheng Z. Removal of heavy metal ions using chitosan and modified chitosan: a review. J Mol Liq, **214**, 175 (2016). https://doi.org/10.1016/j.molliq.2015.12.013.

[46] Fritz W, Schlunder EU. Simultaneous adsorption equilibria of organic solutes in dilute aqueous solution on activated carbon. Chem Eng Sci, **29**, 1279 (1974). https://doi.org/10.1016/0009-2509(74)80128-4.

[47] Hamdaoui O, Naffrechoux E. Modeling of adsorption isotherms of phenol and chlorophenols onto granular activated carbon: part II. models with more than two parameters J Hazard Mater, **147**, 401 (2007). https://doi.org/10.1016/j.jhazmat.2007.01.023.